

Sea-state-dependent wind work on the oceanic general circulation

Guoqiang Liu¹ and William Perrie¹

Received 10 May 2013; accepted 31 May 2013; published 27 June 2013.

[1] We examine sea-state-dependent wind work on the oceanic general circulation, using a wave hindcast dataset, QuikSCAT winds, and geostrophic and total ocean surface currents from (1) AVISO and (2) ECCO2 model products. For wind work on surface geostrophic currents estimated from AVISO or ECCO2, sea-state-dependent wind stress increases an average of 24% (0.17TW) or 23% (0.15TW), compared with estimates that exclude sea state effects. For wind work on the total surface currents, the sea-state-dependent wind stress increases the wind work by about 24% (0.4TW). In terms of spatial distribution, the *increase* in wind power input occurs mainly in high-wind tropical regions and the mid-latitude storm track regions, like the Antarctic Circumpolar Current region, where the relatively rough ocean surface is characterized by young waves and high winds. By comparison, in some regions with relatively low winds and mature ocean waves, there is a slight *reduction* in estimated wind power input. **Citation:** Liu, G., and W. Perrie (2013), Sea-state-dependent wind work on the oceanic general circulation, *Geophys. Res. Lett.*, 40, 3150–3156, doi:10.1002/grl.50624.

1. Introduction

[2] The mechanical energy input to the ocean by winds is a major source for driving the oceanic general circulation and maintaining the abyssal stratification [e.g., Ferrari and Wunsch, 2009]. Wind work on the ocean is also a fundamental quantitative indicator of the interactions between the atmosphere and ocean. The mean mechanical energy input from wind to the global quasi-steady oceanic general circulation can be estimated from, e.g., Wang and Huang [2004] and Huang [2010] as

$$P = \iint \overline{\boldsymbol{\tau} \cdot \mathbf{v}_s} ds \quad (1)$$

where $\boldsymbol{\tau}$ is the wind stress, surface current $\mathbf{v}_s = \mathbf{v}_g + \mathbf{v}_{ag}$, \mathbf{v}_g is the surface geostrophic current, \mathbf{v}_{ag} is the surface ageostrophic current (Surface Ekman current), the over bar denotes a time average, and $\iint \cdot ds$ represents integration over the global oceans. The first component $P_g = \iint \overline{\boldsymbol{\tau} \cdot \mathbf{v}_g} ds$ is the wind work on the surface geostrophic current, which is believed to be of vital importance for deep-ocean mixing. It is estimated as about 0.76–0.93 TW [e.g. Wunsch, 1998; Huang et al., 2006; Hughes and Wilson, 2008]. The second component $P_{ag} = \iint \overline{\boldsymbol{\tau} \cdot \mathbf{v}_{ag}} ds$ is the wind work on the surface ageostrophic

current, previously estimated as about 0.5–0.7 TW over the near-inertial frequency band [Alford, 2003; Watanabe and Hibiya, 2002], and about 2.4 TW for the sub-inertial frequency band [Wang and Huang, 2004]. The wind power input to the ageostrophic currents is mainly dissipated in the upper ocean. Based on equation (1), Huang et al. [2006] estimated that the wind work on the total surface currents is 1.16 TW, using a coarse resolution model for surface currents, while Von Storch et al. [2007] suggested a value of about 3.8 TW, using estimates from an eddy-resolving model with a very shallow uppermost layer (5 m), for surface currents. These estimates depend essentially on accurate expressions for wind stress. Scott and Xu [2009] reported that the errors in estimating wind work on the general circulation are dominated by wind stress uncertainty. Presently, general circulation models (GCMs) often take the surface wind stress, exerted by the atmosphere on the ocean, as a function of wind alone, written as

$$\boldsymbol{\tau} = \rho_a C_D |\mathbf{U}_a| \mathbf{U}_a \quad (2)$$

where \mathbf{U}_a is the 10 m atmospheric wind, ρ_a is the density of air at sea level, and C_D is the drag coefficient, which is often taken as a constant, or depends on wind speed only. On one hand, the bulk parameterization in equation (2) neglects the dependence of $\boldsymbol{\tau}$ on surface ocean currents in calculations of the wind stress. Although the current speed is thought to be much smaller than wind speed, Duhaut and Straub [2006] showed that neglecting surface ocean currents could reduce the estimate for the wind work on the surface geostrophic circulation by 20%–35% (hereafter, the *DS* effect). For the North Pacific, the *DS* effect reduces the wind work by 27% [Dawe and Thompson, 2006], and for the eddy-rich Gulf Stream region of the northwest North Atlantic, by 17% [Zhai and Greatbatch, 2007].

[3] On the other hand, the drag coefficient C_D itself varies not only with wind speed, but also with the sea surface roughness, as determined by the sea state (wave age or wave steepness) [e.g., Taylor and Yelland, 2001; Drennan et al., 2005; Oost et al., 2002]. Generally, for wind speeds greater than about 5 m/s, ocean surface waves are an important factor in the surface roughness of the ocean, which in turn affects the wind stress [e.g. Drennan et al., 2003]. Experiments show that C_D can vary by up to 50% depending on different sea states at a fixed location [Donelan et al., 1995]. Over the global oceans, on average, Liu et al. [2011] found that sea state effects on C_D can account for 14% of its variation.

[4] Although wind-generated surface waves are thought to be dissipated within the upper mixed layer and cannot directly feed into the general circulation [Agrawal et al., 1992], it is apparent that ocean surface waves can influence the wind work on the general ocean circulation by modifying the surface roughness and, therefore, the momentum transfer. This present paper investigates the effects of sea-state (surface ocean waves) on wind work on the oceanic general circulation, using the ECCO2 products (ftp://ecco2.jpl.nasa.

¹Fisheries and Oceans Canada, Bedford Institute of Oceanography, Dartmouth, Nova Scotia, Canada.

Corresponding author: W. Perrie, Bedford Institute of Oceanography, 1 Challenger Drive, P. O. Box 1006, Dartmouth, NS B2Y 4A2, Canada. (William.Perrie@dfo-mpo.gc.ca)

gov/data1/cube/cube92/; Estimating the Circulation and Climate of the Ocean, Phase II), altimetry surface geostrophic currents, and scatterometer winds.

2. Data and Method

[5] In present study, we use QuikSCAT scatterometer 10 m neutral wind data \mathbf{U}_{10} to calculate surface wind stress. The scatterometer naturally measures the relative motion \mathbf{U}_{10} between the wind vector \mathbf{U}_a and the total surface current \mathbf{V}_S [Kelly *et al.*, 2001], where $\mathbf{U}_{10} = \mathbf{U}_a - \mathbf{V}_S$. Thus, the surface current \mathbf{V}_S impacts on the wind vectors \mathbf{U}_a are implicitly included in the scatterometer winds \mathbf{U}_{10} . Here, daily $1/4^\circ$ latitude-longitude gridded QuikSCAT data (3 day moving averages) and 10 m neutral winds from September 1999 to August 2008 are used. We use recent parameterizations for the momentum roughness length z_0 by Fan *et al.* [2012] to calculate the wind stress, including the effects of the sea state. Assuming that mean wind profile is close to logarithmic, it is written as

$$u_z = u_* / \kappa \ln(z/z_0) \quad (3)$$

where u_z is wind speed at the reference height z , u_* is the friction velocity at the air side, and $\kappa = 0.4$ is the Von Karman constant. From field data studies [Drennan *et al.*, 1996, 2003; French *et al.*, 2007; Powell *et al.*, 2003] it follows that

$$z_{ch} = z_0 g / u_*^2 = m (c_p / u_*)^n \quad (4)$$

where $m = 0.023 / 1.0568^{|\mathbf{U}_{10}|}$ and $n = 0.012 |\mathbf{U}_{10}|$ [Fan *et al.*, 2012]. Here, c_p / u_* is wave age, where c_p the phase speed of the waves at the spectral peak and u_* is the friction velocity at the air-water interface. For neutral stratification, the drag coefficient has a one-to-one correspondence with the roughness length through the relation

$$C_D = \kappa^2 [\ln(z/z_0)]^{-2}. \quad (5)$$

[6] We solve equations (3) and (4) together with equation (5) at $z = 10$ m to obtain C_D . To calculate wind stress, we need air density $\rho_a = 1.223 \text{ kg m}^{-3}$, \mathbf{U}_{10} , and c_p . Here c_p is computed from the deep water (linear) dispersion relation $c_p = g / 2\pi f_p$, where f_p is the frequency of the waves at the spectral peak. Related studies using ocean surface waves have been restricted by the spatial limitations of buoy data, which are sparse point locations, concentrated in coastal areas, and also by the temporal and spatial resolution limitations of satellite altimeter data, which have only been available since the late 1980s, and have tens of kilometers separating consecutive tracks. To counteract these limitations, spectral wave models have been developed in recent decades and have reached a sufficiently high level of accuracy that they can provide reliable estimates for H_s (significant wave height) and T_p (peak wave period) with errors of the order of 20% [e.g. Bidlot *et al.*, 2001; Raschle *et al.*, 2008].

[7] Therefore, in the present study, we use a well-validated global hindcast of wave parameters, constructed for geophysical applications from WAVEWATCH III, available at <ftp://ftp.ifremer.fr/ifremer/cersat/>, with newly developed wind sea and swell dissipation source terms [Ardhuin *et al.*, 2010]. The wave hindcast database has been shown to have relatively high accuracy, using these new source term

parameterizations. The temporal and spatial resolutions are required to be within 3 h and 0.5° , respectively, using a spectral grid with 24 directions and 31 frequencies, spaced from 0.037 to 0.72 Hz. In order to estimate the wind work on surface geostrophic currents, two surface geostrophic currents data sets are used. One is AVISO “Update” absolute geostrophic velocity data. AVISO data are provided as daily averages on a $1/3^\circ$ longitude Mercator grid. The altimeter products were produced by Ssalto/Duacs and distributed by AVISO, with support from Cnes (<http://www.aviso.oceanobs.com/duacs/>). The second is diagnosed from ECCO2 model-based sea surface height data, using geostrophy. Because geostrophy is not applicable at the equator, a latitudinal region of $\pm 3^\circ$ is excluded. The surface current data is obtained from the ECCO2, from the uppermost model layer (5 m). ECCO2 products have $1/4^\circ$ latitude-longitude spatial resolution and use temporal averages of 1 day for sea surface height and 3 days for surface currents.

[8] As a baseline comparison, the wind work is also calculated using a wind stress with wind-only dependency, based on Large *et al.* [1994]. To calculate the wind work using equation (1), the AVISO geostrophic currents and related wave parameters are re-gridded (using bilinear interpolation) to the $1/4^\circ$ latitude-longitude grid used by scatterometer data, and ECCO2.

3. Results

[9] Following equation (1), the wind work on the surface geostrophic currents is calculated as the dot-product of the QuikSCAT scatterometer wind stress with the sea-state-dependent drag coefficient and surface geostrophic currents from (a) altimetry (P_{g_AVISO}) and (b) ECCO2 sea surface height (P_{g_ECCO2}). For P_{g_AVISO} , this approach results in an estimate of 0.88 TW; however, if the $\pm 3^\circ$ latitudinal band on both sides of the equator is excluded, the estimate is reduced to 0.81 TW. For the corresponding only-wind-dependent wind stress, these wind power input estimates are 0.71 TW, and 0.65 TW, respectively. These values are slightly smaller than those calculated by Hughes and Wilson [2008], possibly because of the high frequency variability of the daily geostrophic current, which is used in the present study. For P_{g_ECCO2} , estimates are 0.81 TW and 0.66 TW with and without the effects of sea state. Figures 1a and 1b and Figures 2a and 2b show the distributions of the wind work, averaged over 10 years, on the surface geostrophic currents for P_{g_AVISO} and P_{g_ECCO2} , with and without the effects of sea state. In both cases, the spatial patterns are consistent with those found in previous estimates [e.g., Wunsch, 1998; Hughes and Wilson, 2008], with most of the wind power contribution occurring in the Southern Ocean, accounting for about two thirds of the total (more than 60%). Moreover, for P_{g_AVISO} , the maximum in the Southern Ocean reaches $50 \times 10^{-3} \text{ W/m}^2$ in the sea-state-dependent case, while for P_{g_ECCO2} , the maximum is $55 \times 10^{-3} \text{ W/m}^2$. For the sea-state dependent wind stress minus the wind-only dependent wind stress, the differences in magnitudes are shown in Figures 1c and 2c.

[10] Clearly, the positive power input is greatly enhanced in the Southern Ocean, contributing more than 75%, or about 0.14 TW of the total increase for P_{g_AVISO} . For P_{g_ECCO2} , the contribution is also more than 75%, or about 0.11 TW. In some areas of the extra-tropical oceans, for example the

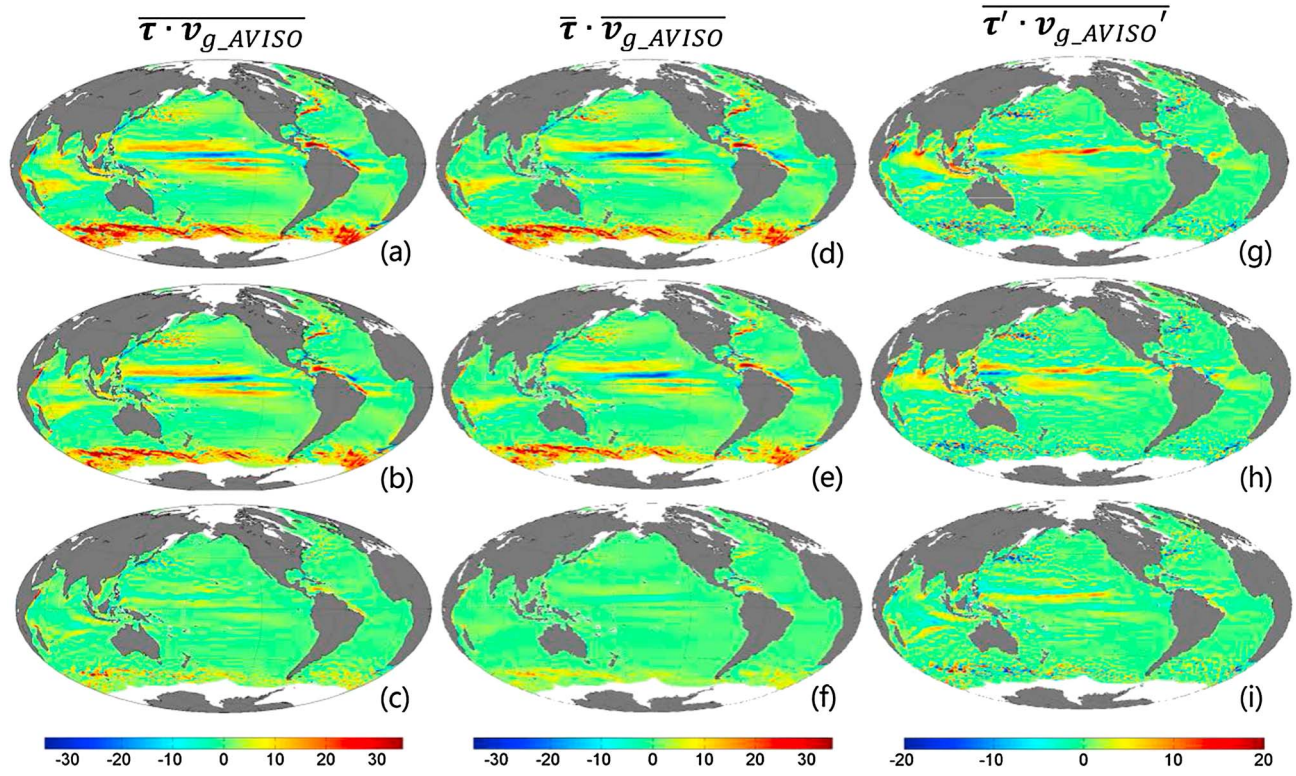


Figure 1. (a) Ten-year *mean* P_{g_AVISO} with sea-state dependent wind stress, (b) same as Figure 1a calculated with only wind-dependence wind stress, and (c) 10-year *mean* P_{g_AVISO} as in data in Figure 1a minus data in Figure 1b; (d–f) data are the same as in Figures 1a–1c but for $\overline{P_{g_AVISO}}$; (g–i) data are the same as in Figures 1a–1c but for P'_{g_AVISO} . Units are 10^{-3} Wm^{-2} .

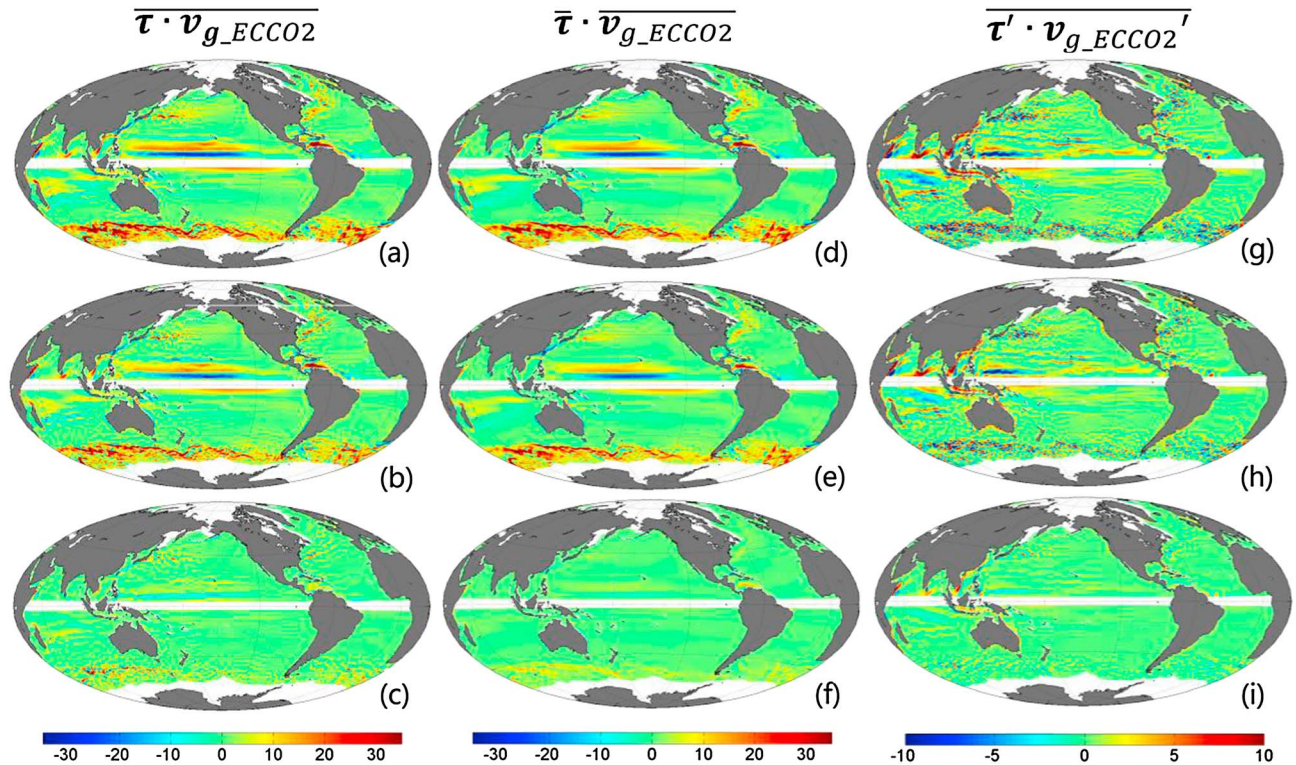


Figure 2. (a) Ten-year *mean* P_{g_ECCO2} with sea-state dependent wind stress, (b) same as Figure 2a calculated with only wind-dependence wind stress, and (c) 10-year *mean* P_{g_ECCO2} as in data in Figure 2a minus data in Figure 2b; (d–f) data are the same as in Figures 2a–2c but for $\overline{P_{g_ECCO2}}$; (g–i) data are the same as in Figures 2a–2c but for P'_{g_ECCO2} . Units are 10^{-3} Wm^{-2} .

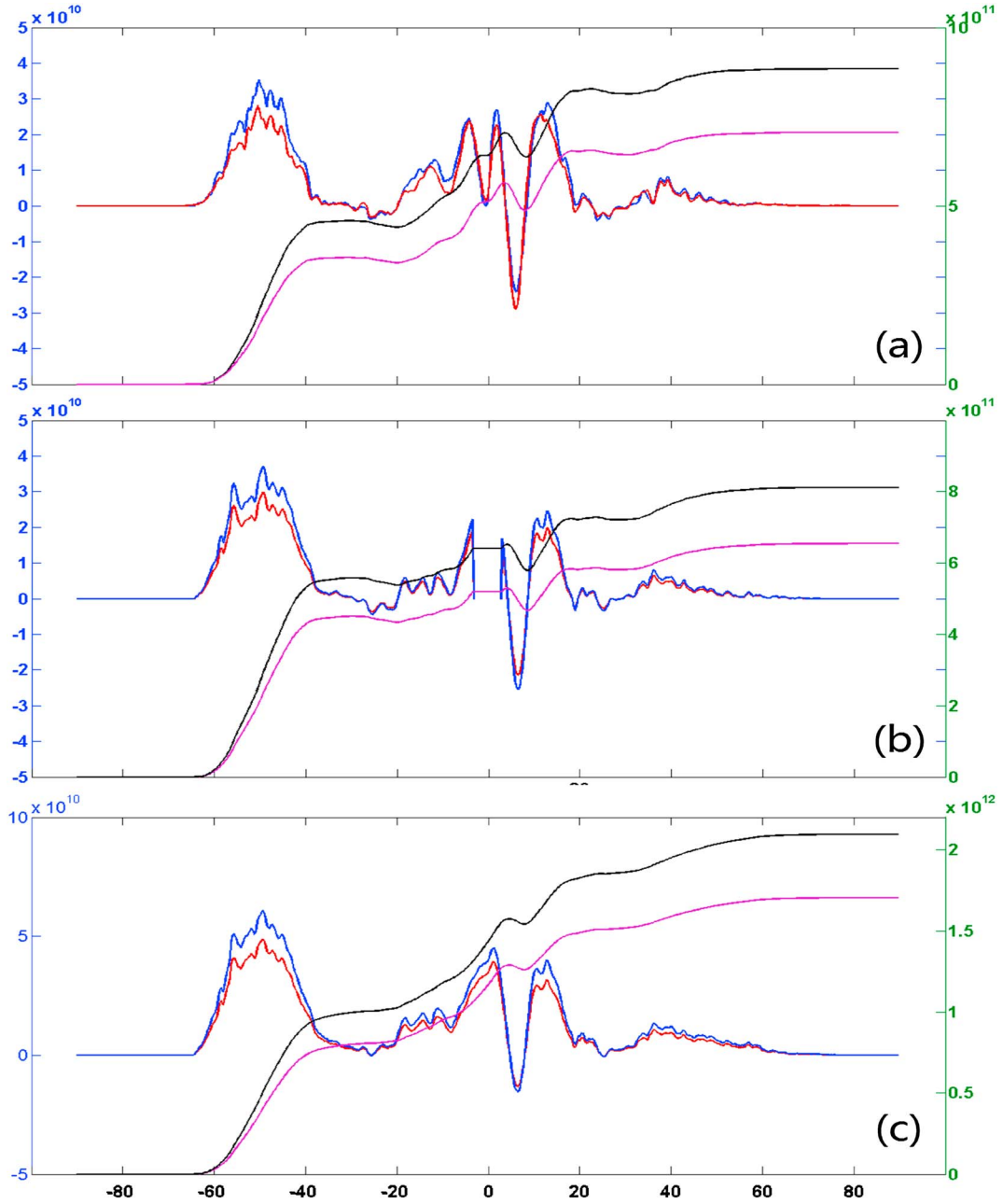


Figure 3. (a) Zonal integral of wind work on surface geostrophic current P_{g_AVISO} . Blue line is latitude integral *with* sea-state-dependent wind stress (W/degree, along the longitude); red line is *with* wind-only-dependent wind stress (W/degree); black line is cumulative integral, starting *from* the southern boundary, *with* sea-state-dependent wind stress; and purple line is *with* wind-only-dependent wind stress. Left vertical axis is for blue and red lines, and right vertical axis is for black and purple lines. Units: W. (b) Data are the same as in Figure 3a but for P_{g_ECCO2} . (c) Data are the same as in Figure 3a but for P_s .

Gulf Stream and Kuroshio Extension regions, both positive and negative wind work are more notable when the effects of sea state on wind stress are included. This is also indicated in zonal and cumulative integrals of wind work in Figures 3a and 3b. Integrated globally, the sea-state-dependent wind stress increases the wind work on the geostrophic ocean circulation by about 24%, from 0.71 TW to 0.88 TW for P_{g_AVISO} , whereas for P_{g_ECCO2} , the increase is about 23%, from 0.66 TW to 0.81 TW.

[11] Therefore, the sea state effect on wind work is comparable to the *DS* effect, which tends to reduce the wind work on the oceanic general circulation. Furthermore, in order to

examine the contributions of mean and time-dependent wind work on the surface geostrophic current, as well as the effects of sea-state, P_g may be written as

$$P_g = \iint \bar{\boldsymbol{\tau}} \cdot \bar{\mathbf{v}}_g ds + \iint \overline{\boldsymbol{\tau}' \cdot \mathbf{v}'_g} ds. \quad (6)$$

[12] The first term on the right side denotes the *mean* wind work \bar{P}_g done by the *mean* wind stress $\bar{\boldsymbol{\tau}}$ on the *mean* surface geostrophic current $\bar{\mathbf{v}}_g$, while the second term is the time-dependent wind power input P'_g . The primed fluctuation $\boldsymbol{\tau}'$ is taken relative to the time mean of the wind stresses,

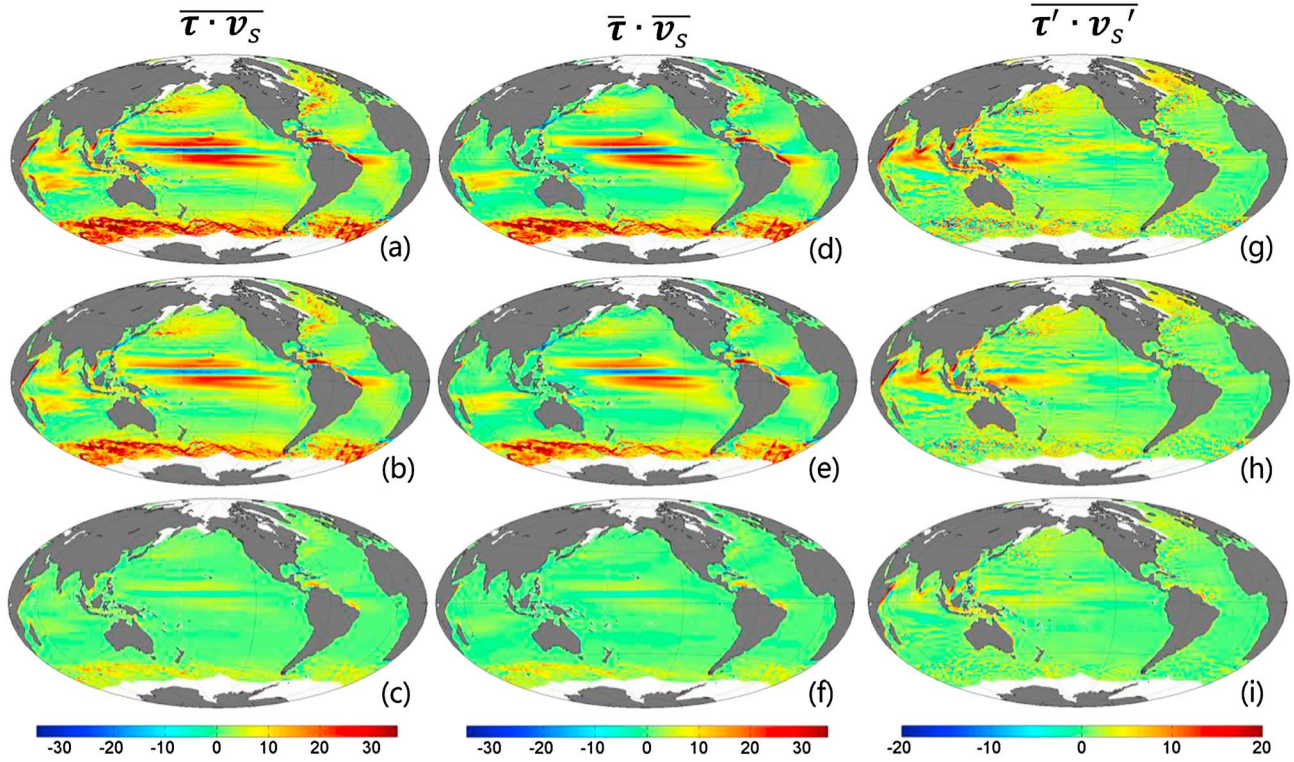


Figure 4. (a) Ten-year mean P_s with sea-state dependent wind stress, (b) same as Figure 4a calculated with only wind-dependence wind stress, and (c) 10-year mean P_s as in data in Figure 4a minus data in Figure 4b; (d–f) data are the same as in Figures 4a–4c but for $\overline{P_s}$; (g–i) data are the same as in Figures 4a–4c but for P'_s . Units are 10^{-3} Wm^{-2} .

and \mathbf{v}'_g represents the surface geostrophic current anomalies (mesoscale eddies). P'_g is evaluated from the difference between P_g and $\overline{P_g}$. Using the mean wind stress and mean AVISO surface geostrophic current, the mean wind work ($\overline{P_{g_AVISO}}$) is 0.85 TW. However, excluding the effects of waves, the corresponding value is 0.69 TW, as shown in Figures 1d and 1e. As for mean wind stress and the ECCO2 surface geostrophic current, the mean wind work ($\overline{P_{g_ECCO2}}$) is 0.77 TW and 0.65 TW, respectively, with and without the effects of sea state, as shown in Figures 2d and 2e. The dominance of the mean contributions of $\overline{P_{g_AVISO}}$ and $\overline{P_{g_ECCO2}}$ is similar and consistent with previous estimates [e.g., Wunsch, 1998]. Globally, consideration of sea state results in an increase of 0.16 TW, or 23%, for $\overline{P_{g_AVISO}}$, while for $\overline{P_{g_ECCO2}}$, the increase is about 0.14 TW, or 21%.

[13] Figures 1f and 2f suggest that the sea-state-dependent wind stress causes a significant enhancement in the wind work, particularly in the mid-latitude storm track regions, the Southern Ocean from 35°S to 60°S, and the Gulf Stream and Kuroshio Extension areas. These areas correspond to relatively high winds and young waves, suggesting that more momentum is available to the waves and that the sea surface is rougher than in other regions. This result is also consistent with estimates for inverse wave age calculated using the ERA-40 wind and wave data averaged over 1958–2001 by Hanley et al. [2010]. However, there is clearly a slight reduction in wind work that occurs mainly over an elongated region of the tropical North Pacific, as well as subtropical regions of the East Pacific and Atlantic, corresponding to relatively lower winds, more mature ocean waves, and, thus, ocean surfaces that tend to be smoother

than other regions. Figures 1g and 1h and Figures 2g and 2h show the time-dependent contributions to the wind power input, with and without the effects of sea state, for wind work on AVISO (P'_{g_AVISO}) and ECCO2 (P'_{g_ECCO2}) surface geostrophic current anomalies. Both spatial patterns are similar to the results of Scott and Xu [2009]. Global integration shows that the time-dependent wind work is 0.03 TW for P'_{g_ECCO2} . Without the effects of sea state, the values are about 0.021 TW and 0.026 TW, respectively. Over the Southern Ocean, and the Gulf Stream and Kuroshio Extension regions, P'_{g_AVISO} is negative, and therefore, the tropical region dominates the time-dependent wind work. For P'_{g_ECCO2} , the subtropical region is the main positive power input area for some selected regions, e.g., the South China Sea. Figures 1i and 2i show the difference between the two kinds of time-dependent wind work for P'_{g_AVISO} and P'_{g_ECCO2} . There is an increase of only 0.009 TW and 0.014 TW, respectively. Therefore, for P_{g_AVISO} or P_{g_ECCO2} , the mean wind work component occupies 94% or 93%, or about 0.16 TW or 0.14 TW, of the total increase induced by the effects of sea-state-dependent wind stresses.

[14] Figure 4 shows the wind work on the surface current (wind stress on the surface current P_s ; mean wind stress on mean surface currents $\overline{P_s}$; and the wind work on surface current anomalies P'_s) calculated using wind stress, with and without sea state effects, and also surface currents from ECCO2. Integrated globally, the sea-state-dependent wind stress increases the wind work on the surface currents by about 24%, from 1.7 TW to 2.1 TW, and the maximum over $75 \times 10^{-3} \text{ W/m}^2$ is found over the Southern Ocean. $\overline{P_s}$ and P'_s

Table 1. Wind Power Input to the Surface Geostrophic Current and Total Surface Current by Daily QuikSCAT Scatterometer Data With AVISO and ECCO2 Geostrophic Current and ECCO2 Surface Current^a

| P_{g_AVISO} | \overline{P}_{g_AVISO} | P'_{g_AVISO} | P_{g_ECCO2} | \overline{P}_{g_ECCO2} | P'_{g_ECCO2} | P_s | \overline{P}_s | P'_s |
|----------------|---------------------------|-----------------|----------------|---------------------------|-----------------|-------|------------------|--------|
| 0.88 | 0.85 | 0.03 | 0.81 | 0.77 | 0.04 | 2.09 | 1.44 | 0.65 |
| 0.71 | 0.69 | 0.02 | 0.66 | 0.63 | 0.026 | 1.70 | 1.18 | 0.52 |
| 0.17 | 0.16 | 0.01 | 0.15 | 0.136 | 0.014 | 0.39 | 0.26 | 0.13 |

^aRow 1 indicates wind power input *with* the sea-state-dependent wind stress; row 2 indicates the power input *with* only-wind-dependent wind stress; row 3 is the *difference* between row 1 and row 2 (units: TW).

contribute to the total increase of P_s by about 66% (0.26 TW) and 33% (0.13 TW), respectively. The difference in P_s , with and without wave effects, as shown in Figure 4f, suggests that the sea-state-dependent wind stress induces a significant increase on the wind power input to mean surface currents in midlatitude storm track regions and in the Southern Ocean, corresponding to the high winds and young waves that are prevalent in these regions. Consistent with the spatial patterns in Figures 1f and 2f, the reductions in wind work on the surface currents in the tropical North Pacific, as well as in subtropical regions of the Northeast Pacific and Northeast Atlantic, are evident. These regions are characterized by relatively smooth ocean surfaces, owing to lower winds and more mature waves.

4. Discussion and Conclusions

[15] Ocean surface waves are the medium that transfer momentum across the air-sea interface. Generally, wind stress over the ocean surface depends on the sea surface roughness, which is determined by the surface waves. Underdeveloped wind seas are rougher than their fully developed counterparts, resulting in increased C_D , and vice versa. Although sea state can significantly modify C_D , the wind stress computed from only-wind-dependent, or constant C_D , is *often* used for modeling currents or estimating wind work on the oceanic general circulation, which can result in errors. In this study, we present the effects of sea state on wind stress and, therefore, on estimates of wind work on the oceanic general circulation using observed winds and currents, and numerical estimates from models. Table 1 summarizes the various effects of wind work.

[16] There are substantial uncertainties in the datasets and drag coefficient parameterizations that we used. On one hand, besides the errors in the spectral wave and ocean model results, satellite products have errors. For example, for wind speed, the error is about 0.75 m/s in the along-wind direction and 1.50 m/s in the cross wind direction. For wind direction, the error is 14° for winds higher than about 6 m/s [Chelton and Freilich, 2005]. On the other hand, drag coefficient parameterizations are still subject to debate [e.g. Drennan *et al.*, 2005]. However, the uncertainty in estimate of P_{g_AVISO} , due to uncertainty in the surface geostrophic currents, is relatively negligible, within ± 0.01 TW [Scott and Xu, 2009]. By comparison, uncertainties from scatterometer wind and wave data constitute a larger source of error, about ± 0.05 and ± 0.04 TW, respectively, for P_{g_AVISO} and P_{g_ECCO2} , while for P_s , the uncertainties are about ± 0.08 and ± 0.07 TW owing to the uncertainties in scatterometer wind and wave data. In terms of wind stress parameterizations, variations in sea-state-dependent wind stress, ranging from that of Large *et al.* [1994] to the algorithm of Liu and Tang [1996], imply increases of P_{g_AVISO} (P_{g_ECCO2} , P_s) from 0.71 (0.66, 1.70) to

0.75 (0.68, 1.75) TW, suggesting a relatively small uncertainty of about 0.04 (0.02, 0.05) TW. For sea-state-dependent wind stress, comparing the method of Fan *et al.* [2012] to the algorithm proposed by Drennan *et al.* [2003], we find that P_{g_AVISO} (P_{g_ECCO2} , P_s) increases from 0.88 (0.81, 2.09) to 0.91 (0.83, 2.14) TW, an uncertainty of about 0.03 (0.02, 0.05) TW.

[17] Accuracy depends on the data and method used. Our methodology for estimating the sea state contribution to wind work is based on concurrent scatterometer wind and oceanic current data and is therefore generic and robust. The increase of 25% (or 23%), or about 0.17 (0.15) TW for AVISO (ECCO2) surface geostrophic currents, is significant when taking account of the effects of sea state. It means that more wind power will drive the large-scale circulation and feed deep-ocean mixing. For wind work on the total surface current from ECCO2, there is a significant increase of about 24%, or about 0.4TW, due to sea state effects.

[18] Therefore, the contribution to the large-scale ocean circulation due to sea state effects is comparable to the DS effect on wind work, which implies a negative bias on the wind work by about 20%–35%. Therefore, our conclusion is that analysis winds, like NCEP or CFSR datasets, may perform better, as forcing fields, for an ocean-only model, than QuikSCAT scatterometer data, which potentially contain the DS effect. Moreover, when scatterometer data is used, both the DS effect and the sea state influence should be taken into consideration in order to avoid underestimating the wind work on ocean circulation. However, in the cases where ocean-only models are used, without the sea-state-dependent wind stress, results may include significant errors and lead to underestimates in the intensity owing to a *reduction* of 0.17 (0.15) TW energy input to the deep ocean. Thus, results may fail to achieve accurate spatial patterns for the large-scale ocean circulation and underestimate the intensity of the meridional overturning circulation, which needs 2 TW to turbulently warm the abyssal waters so that upwelling can occur [Munk and Wunsch, 1998]. We suggest that accurate coupled ocean-wave-atmosphere models, in which both sea-state and DS effects are taken into consideration, may be able to address these issues for large-scale circulation simulations.

[19] **Acknowledgments.** We thank two anonymous reviewers. This paper is supported by the Canadian Panel on Energy Research and Development, the National Ocean Partnership Program, and the Aquatic Climate Change Adaptation Services Program.

References

- Agrawal, Y. C., E. A. Terray, M. A. Donelan, P. A. Hwang, A. J. Williams III, W. M. Drennan, K. K. Kahma, and S. A. Kitaigorodskii (1992), Enhanced dissipation of kinetic energy beneath surface waves, *Nature*, 359, 219–220.
- Alford, M. H. (2003), improved global maps and 54-year history of wind work on ocean inertial motions, *Geophys. Res. Lett.*, 30(8), 1424, doi:10.1029/2002GL016614.

- Ardhuin, F., et al. (2010), Semi-empirical dissipation source functions for wind-wave models: Part I, definition, calibration and validation, *J. Phys. Oceanogr.*, *40*(9), 1917–1941.
- Bidlot, J.-R., et al. (2001), Intercomparison of operational wave forecasting systems, *10th International Workshop on Wave Hindcasting and Forecasting and Coastal Hazard Symposium*, Nov 11–16, pp. 22, U.S. Army Engineer Research and Development Centre's Coastal and Hydraulics Laboratory, and Environmental Canada, jointly with the WMO and IOC through the Joint WMO/IOC Technical Commission for Oceanography and Marine Meteorology (JCOMM), North Shore, Oahu, Hawaii.
- Chelton, D. B., and M. H. Freilich (2005), Scatterometer-based assessment of 10 m wind analyses from the operational ECMWF and NCEP numerical weather prediction models, *Mon. Weather Rev.*, *133*, 409–429.
- Dawe, J. T., and L. Thompson (2006), Effect of ocean surface currents on wind stress, heat flux, and wind power input to the ocean, *Geophys. Res. Lett.*, *33*, L09604, doi:10.1029/2006GL025784.
- Donelan, M. A., F. W. Dobson, S. D. Smith, and R. J. Anderson (1995), Reply, *J. Phys. Oceanogr.*, *25*, 1908–1909.
- Drennan, W. M., M. A. Donelan, E. A. Terray, and K. B. Katsaros (1996), Oceanic turbulence dissipation measurements in SWADE, *J. Phys. Oceanogr.*, *26*, 808–815.
- Drennan, W. M., G. C. Graber, D. Hauser, and C. Quentin (2003), On the wave age dependence of wind stress over pure wind seas, *J. Geophys. Res.*, *108*(C3), 8062, doi:10.1029/2000JC000715.
- Drennan, W. M., P. K. Taylor, and M. J. Yelland (2005), Parameterizing the sea surface roughness, *J. Phys. Oceanogr.*, *35*, 835–848.
- Duhaut, T. H., and D. N. Straub (2006), Wind stress dependence on ocean surface velocity: implications for mechanical energy input to ocean circulation, *J. Phys. Oceanogr.*, *36*, 202–211.
- Fan, Y., S.-J. Lin, I. M. Held, Z. Yu, and H. L. Tolman (2012), Global ocean surface wave simulation using a coupled atmosphere–wave model, *J. Clim.*, *25*, 6233–6252.
- Ferrari, R., and C. Wunsch (2009), Ocean circulation kinetic energy: reservoirs, sources, and sinks, *Annu. Rev. Fluid Mech.*, *41*, 253–282.
- French, J. R., W. M. Drennan, and J. A. Zhang (2007), Turbulent fluxes in the hurricane boundary layer. Part I: Momentum flux, *J. Atmos. Sci.*, *64*, 1089–1102.
- Hanley, K. E., S. E. Belcher, and P. P. Sullivan (2010), A global climatology of wind-wave interaction, *J. Phys. Oceanogr.*, *40*, 1263–1282.
- Huang, R. X. (2010), *Ocean Circulation: Wind-Driven and Thermohaline Processes*, 806 pp., Cambridge Univ. Press, New York.
- Huang, R. X., W. Wang, and L. Liu (2006), Decadal variability of wind-energy input to the world ocean, *Deep Sea Res.*, *53*, 31–41.
- Hughes, C. W., and C. Wilson (2008), Wind work on the geostrophic circulation: an observational study of the effect of small scales in the wind stress, *J. Geophys. Res.*, *113*, C02016, doi:10.1029/2007JC004371.
- Kelly, K. A., S. Dickinson, M. J. McPhaden, and G. C. Johnson (2001), Ocean currents evident in satellite wind data, *Geophys. Res. Lett.*, *28*, 2469–2472, doi:10.1029/2000GL012610.
- Large, W. G., J. C. McWilliams, and S. C. Doney (1994), Oceanic vertical mixing: A review and a model with a nonlocal boundary layer parameterization, *Rev. Geophys.*, *32*, 363–403.
- Liu, W. T., and W. Tang (1996), Equivalent neutral wind, *JPL Publ.*, *96-17*, 16 pp., Jet Propul. Lab., Pasadena, Calif.
- Liu, G., Y. He, H. Shen, and J. Guo (2011), Global drag coefficient estimates from scatterometer wind and wave steepness, *IEEE Trans. Geosci. Remote Sens.*, *49*(5), 1499–1503.
- Munk, W., and C. Wunsch (1998), Abyssal recipes II. Energetics of tidal and wind mixing, *Deep Sea Res.*, *45*, 1977–2010.
- Oost, W. A., G. J. Komen, C. M. J. Jacobs, and C. van Oort (2002), New evidence for a relation between wind stress and wave age from measurements during ASGAMAGE, *Boundary Layer Meteorol.*, *103*, 409–438.
- Powell, M. D., P. J. Vickery, and T. Reinhold (2003), Reduced drag coefficient for high wind speeds in tropical cyclones, *Nature*, *422*, 279–283.
- Rascle, N., F. Ardhuin, P. Queffelec, and D. Croizé-Fillon (2008), A global wave parameter database for geophysical applications. Part I: wave-current-turbulence interaction parameters for the open ocean based on traditional parameterizations, *Ocean Model.*, *25*, 154–171.
- Scott, R. B., and Y. Xu (2009), An update on the wind power input to the surface geostrophic flow of the World Ocean, *Deep Sea Res.*, *56*, 295–304.
- Taylor, P. K., and M. J. Yelland (2001), The dependence of sea surface roughness on the height and steepness of the waves, *J. Phys. Oceanogr.*, *31*(2), 572–590.
- von Storch, J.-S., H. Sasaki, and J. Marotzke (2007), Wind-generated power input to the deep ocean: an estimate using a $1/10^\circ$ general circulation model, *J. Phys. Oceanogr.*, *37*, 657–672.
- Wang, W., and R. X. Huang (2004), Wind energy input to the Ekman layer, *J. Phys. Oceanogr.*, *34*, 1267–1275.
- Watanabe, M., and T. Hibiya (2002), Global estimates of the wind-induced energy flux to inertial motions in the surface mixed layer, *Geophys. Res. Lett.*, *29*(8), 1239, doi:10.1029/2001GL014422.
- Wunsch, C. (1998), The work done by the wind on the oceanic general circulation, *J. Phys. Oceanogr.*, *28*, 2332–2340.
- Zhai, X., and R. J. Greatbatch (2007), Wind work in a model of the northwest Atlantic Ocean, *Geophys. Res. Lett.*, *34*, L04606, doi:10.1029/2006GL028907.